Debye temperature, anharmonic thermal motion and oxygen non-stoichiometry in yttria stabilized cubic zirconia

1998 J. Phys.: Condens. Matter 10 3823

(http://iopscience.iop.org/0953-8984/10/17/013)

J. Phys.: Condens. Matter **10** (1998) 3823–3832. Printed in the UK PII: S0953-8984(98)89812-3

Debye temperature, anharmonic thermal motion and oxygen non-stoichiometry in yttria stabilized cubic zirconia

Erich Kisi and Ma Yuxiang

Department of Mechanical Engineering, The University of Newcastle, NSW 2308, Australia

Received 4 December 1997

Abstract. The temperature dependence of the Debye–Waller factors of a 9.4 mol% Y_2O_3 stabilized cubic ZrO_2 ceramic was studied in the range 4–1923 K using neutron powder diffraction. It was found that the data could not be modelled on a harmonic Debye-like model with an additive static disorder component but are significantly anharmonic. The anharmonic thermal motion in this material is not confined to the usual fluorite third-order term for the anion. It is shown that the temperature variation of the Debye–Waller factors is well modelled by an isotropic fourth-order anharmonic vibration of both the cation and anion each with its own additive static disorder component. The Debye temperature was determined as approximately 963 K which is much higher than the only known previous measurement. There is evidence that the sample became non-stoichiometric during the measurements. The oxygen content appears to follow an extrapolation of the ZrO_{2-x} lower phase boundary of the Zr–O phase diagram.

Zirconia (ZrO_2) has three ambient-pressure polymorphs with fluorite related cubic, tetragonal and monoclinic structures. The monoclinic form is stable to 1443 K, the tetragonal form between 1443 K and 2643 K and the cubic phase above 2643 K. Zirconia phases have been widely utilized in ceramics of various kinds ranging from fast-ion conductors to structural ceramics. The high-temperature phases are stabilized to room temperature by the addition of other oxides such as Y_2O_3, MgO or CaO. Quite large additions of the stabilizer are required to maintain the cubic phase to room temperature (e.g. >8 mol% Y_2O_3) [1]. The addition of stabilizing oxides induces a number of complex local structural changes including substitutional cations, vacant oxygen sites to maintain charge balance and relaxations of both anions and cations around the vacant oxygen sites and substituent cations. As the temperature is increased, the cubic phase becomes highly conducting due to the high mobility of the O ions and the ready availability of vacant oxygen sites.

Because of the large ion relaxations, diffraction studies of CSZs invariably have large displacement parameters or Debye–Waller factors given by $B = 8\pi^2\langle u^2\rangle$ where $\langle u^2\rangle$ is the mean-square displacement of an ensemble of atoms about the ideal crystallographic position. In its simplest form, it is assumed the atom displacements are spherically distributed about the mean position. The static (disorder) and dynamic (thermal) contributions to B cannot be separated at a single temperature using an elastic diffraction technique (the ergodic principle). However, it has been suggested [2–4] that, given a good model of the temperature variation of B due to thermal vibrations, the temperature dependence of the observed B may be used to separate the magnitude of the average disorder and thermal displacements (unfortunately without reference to directions). This technique has been applied to cubic zirconia previously [4], where it was observed that in a 10 mol% Y_2O_3 ceramic, the rms

0953-8984/98/173823+10$19.50

displacement at 15 K was 0.33 and 0.22 Å for the anion and cation respectively. A simple Debye-like model was used to separate the thermal and static disorder, but unfortunately the limited number of measurements lowered the quality of the result as discussed below. A similar technique has recently been applied to line broadening in EXAFS data taken between 10 K and room temperature [5].

This paper reports the results of neutron powder diffraction measurements taken from a 9.5 mol% Y_2O_3 cubic zirconia sample between 4 and 1923 K. There is significant static disorder at low temperatures in agreement with [4]. However, the temperature dependence of the displacement parameters cannot be modelled as the sum of a Debye-like thermal vibration and an additive static disorder term. To model the experimental results, it is necessary to use a fourth-order anharmonic term, or to allow the static disorder term to decay as a function of temperature.

The sample was prepared by milling a 9.4 mol% Y_2O_3–ZrO_2 powder for 14 hours using a cubic zirconia vial and balls in a Spex 8000 mixer-mill. The milled powder was dry pressed at 100 MPa followed by pre-firing at 1550 °C for 2 hours. Neutron diffraction data were collected on the Medium Resolution Powder Diffractometer (MRPD) at the Australian Nuclear Science and Technology Organization's HIFAR reactor. The sample was heated from room temperature to 1923 K in a series of steps with neutron data collected at constant temperature after each temperature increment. This procedure was repeated during cooling with a further pattern collected at 4 K using a three-stage He displex. Data from the heating part of the cycle indicate that sintering was incomplete until temperatures greater than 1873 K and so the analysis here is focused on data taken during cooling. Raw data are in the form of scans from 4° to 138° 2θ in 0.1° steps using a neutron wavelength of 1.664(2) Å. Each scan took approximately 2 hours.

The sample was single phase and cubic at all temperatures during cooling. A crystal structure model was refined for each temperature using the Rietveld analysis program LHPM [6, 7]. The analysis proceeded by refinement of a second-order polynomial background correction and diffractometer zero error. In the perfect fluorite aristotype, the lattice parameter and displacement parameters are the only free variables. Because of our interest in the thermal behaviour and displacement parameters, the oxygen site occupancy (N_O) was also refined according to two models. In model 1, the occupancy of both the Zr/Y and the O site were refined but they were constrained to conform to a 'charge balance only' vacancy mechanism in which one O vacancy is created for each Y_2O_3 formula unit added. Model 2 constrains the Zr/Y ratio to conform to the known sample stoichiometry, but allows the O occupancy to vary freely. A typical fit is shown in figure 1.

The refined parameters for both structure models and the agreement indices R_{wp} and R_B [6] are given in table 1. The lattice parameters may be used to extract thermal expansion data. Above 773 K the expansion is relatively linear and is well modelled by the expression

$$a = 5.101\,56 + 6.5000 \times 10^{-5} T \tag{1}$$

leading to a linear coefficient of thermal expansion (q to avoid confusion with the force constant α) of $q = 1.258 \times 10^{-5}$ and a volume coefficient of thermal expansion $\chi = 3.774 \times 10^{-5}$. These data agree well with literature values [8] except for a small offset due to uncertainty in the neutron wavelength.

At low temperature, both structure models are the same. The oxygen occupancy, expressed as the number of oxygen ions per cation, refines to a value in excellent agreement with that expected for charge balance. At temperatures of 773 K and above however, the occupancy appears to decline as a function of temperature and the agreement index R_B for model 2 is significantly better than for model 1. This behaviour is summarized in figure 2.

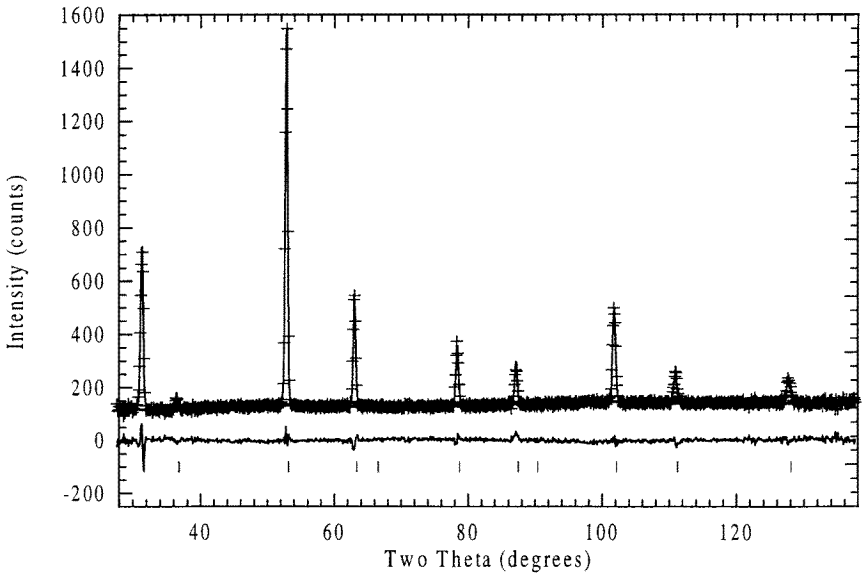

Figure 1. Plotted output from Rietveld refinement of model 2 for the data collected at 1923 K. The raw data are plotted as (+), the calculated profile and difference profile as solid lines and reflection markers as vertical bars below the data.

Table 1. Refined structure and displacement parameters.

	Model 1					Model 2				
T (K)	a (Å)	$B_{Zr/Y}$ (Å^2)	B_O (Å^2)	R_{wp} (%)	R_B (%)	$B_{Zr/Y}$ (Å^2)	B_O (Å^2)	N_O	R_{wp} (%)	R_B (%)
4	5.1298(2)	0.77(4)	2.32(5)	7.0	0.9	0.77(5)	2.32(7)	1.91(2)	7.0	0.9
295	5.1365(2)	1.02(4)	2.53(5)	8.3	1.3	1.02(5)	2.53(7)	1.91(2)	8.3	1.3
773	5.1536(2)	1.08(4)	2.90(8)	7.7	2.8	1.21(7)	2.69(11)	1.82(6)	7.7	2.2
873	5.1597(2)	1.19(5)	3.09(7)	6.6	2.7	1.28(6)	2.96(9)	1.85(3)	6.6	2.4
973	5.1652(2)	1.30(5)	3.22(7)	6.3	2.5	1.41(6)	3.06(9)	1.84(3)	6.3	2.1
1073	5.1710(2)	1.40(5)	3.35(7)	6.1	2.6	1.52(6)	3.17(9)	1.82(3)	6.1	2.1
1173	5.1773(2)	1.50(5)	3.67(7)	6.0	2.2	1.63(6)	3.47(10)	1.82(3)	6.0	1.7
1273	5.1835(2)	1.76(5)	3.84(4)	5.9	2.1	1.86(7)	3.69(10)	1.84(3)	5.9	1.8
1373	5.1905(2)	1.84(5)	4.02(8)	6.1	2.5	2.00(7)	3.76(11)	1.80(3)	6.1	1.9
1423	5.1935(2)	1.95(5)	4.12(8)	6.1	2.4	2.19(7)	3.74(11)	1.76(3)	6.0	1.4
1473	5.1969(2)	1.97(5)	4.23(8)	5.9	1.8	2.09(7)	4.04(11)	1.83(3)	5.9	1.3
1523	5.1998(2)	1.99(5)	4.32(8)	5.8	2.3	2.20(7)	3.99(11)	1.78(3)	5.8	1.4
1573	5.2031(2)	2.03(5)	4.46(9)	5.8	2.2	2.13(7)	4.29(12)	1.84(3)	5.8	1.8
1623	5.2068(2)	2.06(6)	4.38(9)	6.0	2.9	2.28(8)	4.02(12)	1.78(3)	5.4	2.0
1673	5.2097(2)	2.17(6)	4.63(9)	5.8	2.7	2.46(8)	4.13(13)	1.73(3)	5.8	1.5
1723	5.2132(2)	2.34(6)	4.85(9)	5.5	3.2	2.63(8)	4.35(13)	1.73(3)	5.4	2.0
1823	5.2197(2)	2.42(6)	5.15(9)	5.4	3.2	2.68(8)	4.68(13)	1.75(3)	5.3	2.2
1923	5.2265(2)	2.63(6)	5.45(10)	5.1	3.2	2.97(8)	4.84(13)	1.71(3)	4.8	1.9

The solid line indicates the oxygen content derived from a linear extrapolation of the lower phase boundary of ZrO_{2-x} on the Zr–O phase diagram [9, 10]. Whilst the agreement is good, these results should at this stage be treated with caution because of (i) the small number of reflections used in this work (12), (ii) the high correlation coefficient between the oxygen

occupancy and displacement parameters (73%) and (iii) the relatively wide scatter of the data in figure 2. Testing of whether the 'missing' oxygens are localized in the region of $(\frac{1}{2}, \frac{1}{2}, \frac{1}{2})$ resulted in a poorer fit and negative occupancy at $(\frac{1}{2}, \frac{1}{2}, \frac{1}{2})$. In summary, we do have some confidence in model 2, but are unwilling to abandon the conventional wisdom until it has been tested by further work. Hence, in all of the following analyses, B values refined using the stoichiometric structure model 1 were used. Our conclusions are unaltered if B values from model 2 are used although the numerical values of some fitted parameters change slightly.

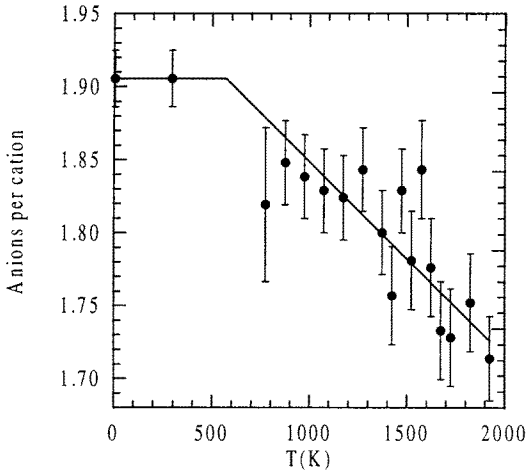

Figure 2. Number of oxygen ions per cation derived from model 2 as a function of temperature (●). The line shows values derived from an extrapolation of the lower phase boundary of ZrO_{2-x} on the Zr–O phase diagram to lower temperatures.

Refinement of the oxygen x co-ordinate, allowing anion displacements along ⟨111⟩ according to a literature model [11] was also conducted. This approximates a third-order anharmonic term (see below) and does not improve the fit at elevated temperatures (e.g. $R_B = 2.9\%$ at 1923 K).

The observed B values are quite large at 4 K (2.3 and 0.8 Å^2 for oxygen and zirconium/yttrium respectively) and can be seen to increase strongly with temperature. The *experimental* value of the mass-weighted mean displacement parameter for a poly-atomic unit cell of k atoms with total mass M, individual masses m_k and individual displacement parameters B_k may be approximated by:

$$B_M = \frac{1}{M}\sum_{1}^{k} m_k B_k. \tag{2}$$

To account for ion relaxation around substitutional Y ions and vacant O sites, we assume they may be modelled with a Gaussian distribution characterized by a 'disorder' displacement parameter B^D which is additive [3, 4]. The observed displacement parameter is then expected to conform to:

$$B_M = B_M^D + B_M^T. \tag{3}$$

In our initial model, the *calculated* value of the thermal part of the displacement parameters B^T relied on the Debye approximation (see for example [11]). For the mass-weighted

average, B_M, the model was modified for a poly-atomic unit cell by using the average mass of an atom in the structure in Debye's original monatomic equation [4].

The Debye model gives a poor fit to the observed displacement parameters (both individual and mass weighted average) due to significant atom displacement at low temperature. A sample fit, forced to agree at high temperature, is shown in figure 3(a). The one variable parameter in this fit, the Debye temperature (θ_D), takes the value 403 K. If a static disorder component is added (equation (3)) a fit similar to figure 3(b) is obtained. It too fits poorly although it gives us a coarse estimate of $B_M^D = 1$ Å^2 representing $\langle u^2 \rangle^{1/2}$, averaged over both cations and anions, of 0.2 Å. For this model to fit would require B_M^D to change with temperature like the dashed line in figure 3(a).

The model may be taken further by assuming that the thermal motion is anharmonic. As a simple approximation, the isolated (average) atom potential for an atom in a cubic material at 0 K may be expanded to fourth order as [12]

$$V = V_0 + \tfrac{1}{2}\alpha u^2 + \beta u_1 u_2 u_3 + \gamma u^4 + \delta(u_1^4 + u_2^4 + u_3^4 - \tfrac{3}{5}u^4) \tag{4}$$

where α, β, γ and δ are force constants, u_1, u_2 and u_3 are the root mean square displacements along the three principal axes and $u^2 = (u_1^2 + u_2^2 + u_3^2)$. The first two terms are the usual harmonic approximation followed by the third-order (anisotropic) and two fourth-order terms (isotropic and anisotropic).

Perfect fluorite structures are known to undergo cubic anharmonic vibration of the anion [12]. The cation has in the past been assumed to behave quasi-harmonically. Rietveld refinement of anion displacement along ⟨111⟩ did not improve the fit indicating that the cubic term for the anion is likely to be small. The cation is geometrically unlikely to execute third-order anharmonic motion and so we may neglect the cubic term. The anisotropic fourth-order term is generally small [12] and so our model consists of the harmonic and isotropic fourth-order terms only. Expansion of an expression for the intensity of a Bragg reflection in a powder pattern leads to:

$$I = S|F|^2 J L A \exp\left(- B^{An} \frac{\sin^2 \theta}{\lambda^2} \right) \tag{5}$$

where S is the scale factor, F the structure factor, J the multiplicity, L the Lorentz factor and A the absorption factor. B^{An} is the anharmonic displacement parameter which, for the restricted case outlined above, is a simple second-order expansion in T given by [12]:

$$B^{An} = B^T(1 + T[2\chi\gamma_G - 20k_B\gamma/\alpha^2]). \tag{6}$$

γ_G is the Grüneisen parameter and χ the volume coefficient of thermal expansion. The term involving these constants represents the quasi-harmonic correction for thermal expansion. There are insufficient intensity data to explicitly incorporate the anharmonic correction into calculated Bragg intensities. We do however have sufficient data to test the temperature dependence predicted by equation (6).

B^D may be included to take account of the disorder component giving:

$$B^{An} = B^D + B^T(1 + T[2\chi\gamma_G - 20k_B\gamma_i/\alpha_i^2]) \tag{7a}$$

for i individual atoms and

$$B_M^{An} = B_M^D + B_M^T(1 + T[2\chi\gamma_G - 20k_B\gamma_M/\alpha_M^2]) \tag{7b}$$

for the mass weighted average. Figure 3(c) shows that the fit to this model is very good for the mass weighted average B and figure 3(d) does likewise for the individual B values. The adjustable parameters in the fitting are the static disorder component B^D, a Debye temperature contained in B^T and the temperature coefficient $C = 2\chi\gamma_G - 20k_B\gamma/\alpha^2$. The

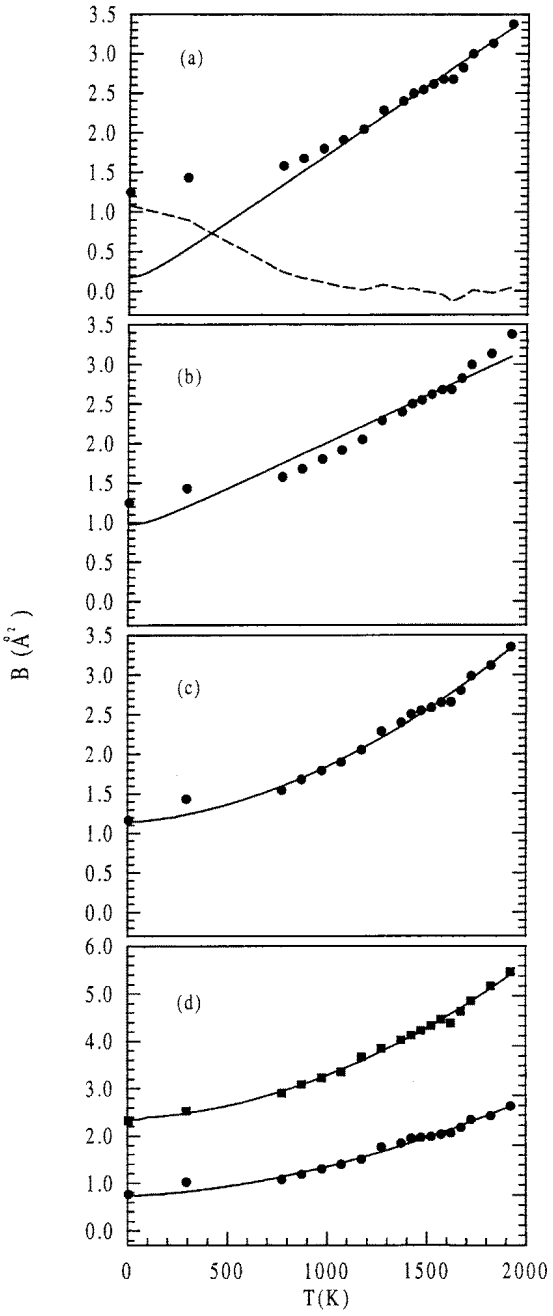

Figure 3. (a) A Debye model B_M^T of the mass weighted average displacement parameter constrained to fit the high-temperature data. Note that there is a substantial disorder component B^D visible at low temperature. The dashed line represents the difference between the calculated and observed values. (b) Fit of $B_M = B_M^T + B_M^D$ to the data. Note the poor agreement, especially at high temperature. (c) Fit of $B_M^{An} = B_M^D + B_M^T(1 + T[2\chi\gamma_G - 20k_B\gamma/\alpha^2])$ to the data for B_M. (d) Fit of $B_{Zr/Y}^{An} = B_{Zr/Y}^D + B_{Zr/Y}^T(1 + T[2\chi\gamma_G - 20k_B\gamma_{Zr}/\alpha_{Zr}^2])$ to $B_{Zr/Y}$, and $B_O^{An} = B_O^D + B_O^T(1 + T[2\chi\gamma_G - 20k_B\gamma_0/\alpha_0^2])$ to B_O.

coefficient C may be decomposed to give the value of γ if χ_1 (known from lattice parameter measurements), γ_G and α are known. The value of α was estimated from the harmonic component making use of

$$\alpha = k_B T / \langle u^2 \rangle \tag{8}$$

and the high-temperature limit of the Debye approximation

$$\langle u^2 \rangle = \frac{3\overline{h}^2 T}{m k_B \theta_D^2} \tag{9}$$

to give

$$\alpha = \frac{m k_B^2 \theta_D^2}{3\overline{h}^2} \tag{10}$$

where $\overline{h}$ is Planck's constant divided by 2π, m is the ionic mass, k_B is Boltzmann's constant and θ_D is the Debye temperature. The Grüneisen parameter, γ_G, was estimated from specific heat data [13] using

$$\gamma_G = \frac{\chi V B_T}{C_V} \tag{11}$$

where χ is the volume coefficient of thermal expansion, C_V is the specific heat at constant volume, V the molar volume and B_T the bulk modulus, calculated from $B_T = E/3(1-2\vartheta)$ using Young's modulus $E = 200$ GPa and Poisson's ratio $\vartheta = 0.27$. A value for C_V of 87.5 J mol^{-1} K^{-1} was used [13] resulting in $\gamma_G = 1.32$. A second method is to use the elastic compliances (from [14]) and the specific heat at constant pressure (C_p) via

$$\gamma_G = \frac{Vq}{C_p(S_{11} + S_{12})} \tag{12}$$

leading to an estimate of $\gamma_G = 1.4$. The average of these values, $\gamma_G = 1.37$, was used in later calculations.

Table 2 contains the values of B^D, $\langle u \rangle^D$, θ_D, α and γ obtained from the fitting procedure for individual ions and for the mass weighted mean.

Table 2. Thermal coefficients and force constants.

Ion	B^D (Å^2)	$\langle u \rangle^D$ (Å)	'θ_D' (K)	α (J m^{-2})	γ (J m^{-4})
Mass weighted mean	1.07	0.12	963	358	-6.46×10^{23}
Zr^{4+}/Y^{3+}	0.70	0.09	694	416	-2.67×10^{23}
O^{2-}	2.3	0.17	1440	302	-1.30×10^{24}

The values for B^D, $\langle u \rangle^D$, α, θ_D and γ are self-consistent in that those for the mass weighted mean are intermediate to the two individual ions. The values of θ_D for the individual ions may be considered as tools for fitting only but have no great physical significance. Our best estimate for the Debye temperature θ_D (963 K) is obtained from fitting the data to equation (7*a*). This is more than 400 K larger than that determined by Argyriou in earlier work [4], apparently because the final point in the restricted data set used for that work appears anomalously low if superimposed on these results. Whilst the exact value should still be regarded with some caution because of the assumptions made in the model, this value of θ_D is considered more precise than the previous one because of the far greater temperature range covered and the smaller temperature interval

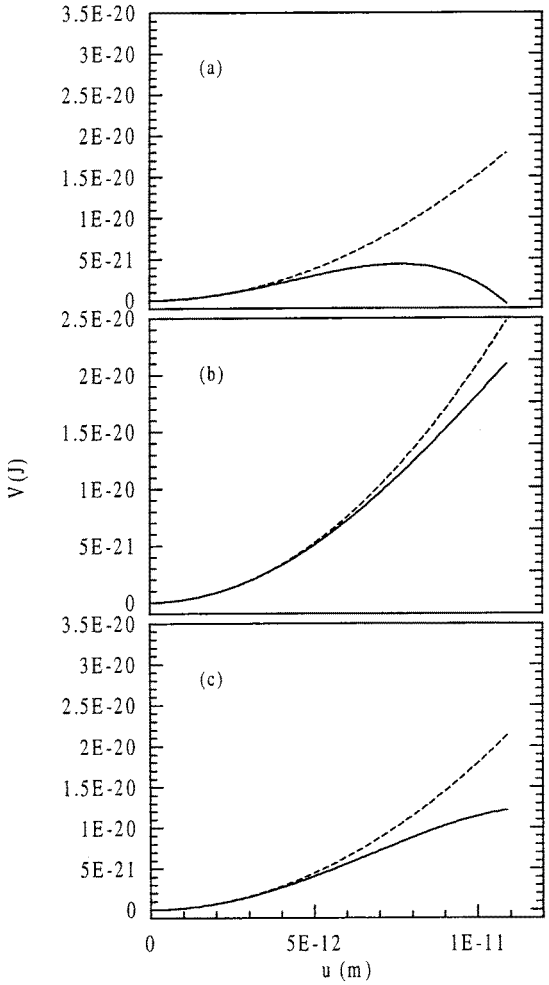

Figure 4. Isolated atom potentials at 0 K calculated for (a) anions, (b) cations and (c) a mass weighted average ion. Solid lines represent the anharmonic model and the dashed lines show the corresponding harmonic components.

between measurements. We know of no other estimates of θ_D for this material for comparison.

The final step in this analysis is to examine the isolated atom potentials generated by the force constants α and γ,

$$V = V_0 + \tfrac{1}{2}\alpha u^2 + \gamma u^4. \tag{13}$$

Figure 4 shows the generated potentials for the individual and mass weighted average fits as well as the corresponding harmonic component $V = V_0 + \frac{1}{2}\alpha u^2$. The apparent departure from harmonic behaviour is very large and must be put into context by recalling the complex local structures in this material. In the current sample, approximately 4.7% of all oxygen sites are vacant at room temperature, possibly rising to >13% at 1923 K if structure model 2 is correct. This means that on average, one expects almost every other unit cell to contain a vacancy at room temperature, possibly rising to almost one per cell at high temperature. The local environment of individual ions is quite different and as such, the concept of

a single characteristic potential for each ion species, as is usual in studies of anharmonic thermal motion, has little validity. In this regard, we feel the use of an isotropic anharmonic correction is well justified, though we believe that no great significance may be attached to the actual potentials derived therefrom.

The validity of structure model 2, indicating greatly reduced oxygen concentration at elevated temperatures, also requires further consideration. First, we may postulate that the 'missing' O ions represent the mobile oxygen ion population responsible for the high ionic conductivity of this material. This would require more O diffusing than there are formal vacancies available, by a factor of approximately 2:1, perhaps making use of the octahedral site ($\frac{1}{2}$, $\frac{1}{2}$, $\frac{1}{2}$) as suggested by the molecular dynamics calculations of Shimojo and Okazaki [15]. This model was tested during the Rietveld refinement procedure and does not appear to fit the data.

Second, the missing O may genuinely represent increasing non-stoichiometry with increasing temperature. The zirconium–oxygen phase diagram [9, 10] shows extensive non-stoichiometry of the cubic phase at temperatures between 1750 and 3000 K which demonstrates the stable existence of lower valence states of zirconium. Similar lower valence states occur in the thorium–oxygen, titanium–oxygen and cerium–oxygen systems. It is not known what effect the addition of Y_2O_3 has on the formation of lower valence states in zirconia; however in general the effect is to depress the phase boundaries to lower temperature and our data appear to lie on an extrapolation of the lower phase boundary. We have no independent measure of the oxygen concentration for comparison.

In closing, it should be noted that it was our intention to use these results to make contact with computational (lattice statics and molecular dynamics) and experimental (neutron and x-ray scattering, EXAFS) studies of the ion relaxations in cubic zirconia. However during the compilation of a recent review [16] general disagreement over the precise local structures in this material became apparent. Should the additional oxygen vacancies suggested by model 2 be confirmed in later work, much of the computational and modelling work based on a fixed stoichiometry will need to be re-evaluated.

Acknowledgments

The authors wish to thank the Australian Research Council and the Australian Institute of Nuclear Science and Engineering for their support. Ma Yuxiang is grateful for a University of Newcastle Research Scholarship. The assistance of Dr Shane Kennedy in recording the neutron data and Professor G E Murch in general discussions were invaluable.

References

[1] Green D J, Hannink R H J and Swain M V 1988 *Transformation Toughening of Ceramics* (Boca Raton, FL: Chemical Rubber Company)
[2] Housley R M and Hess F 1966 *Phys. Rev.* **146** 517
[3] Cheary R W 1991 *Acta Crystallogr.* B **47** 325
[4] Argyriou D N 1994 *J. Appl. Crystallogr.* **27** 155
[5] Li P, Chen I-W and Penner-Hahn J E 1993 *Phys. Rev.* B **48** 10 082
[6] Wiles D B and Young R A 1981 *J. Appl. Crystallogr.* **14** 149
[7] Hill R J and Howard C J 1986 *Australian Atomic Energy Commission Report* AAEC/M112
[8] Tereblanche S P 1989 *J. Appl. Crystallogr.* **22** 283
[9] Ackermann R J, Garg S P and Rauh E G 1977 *J. Am. Ceram. Soc.* **60** 341
[10] Rauh E G and Garg S P 1980 *J. Am. Ceram. Soc.* **63** 239
[11] Howard C J, Hill R J and Reichert B E 1988 *Acta Crystallogr.* B **44** 116

[12] Willis B T M and Pryor A W 1975 *Thermal Vibrations in Crystallography* (Cambridge: Cambridge University Press)
[13] Touloukian Y S (ed) 1979 *Specific Heat: Non-metallic Solids (Thermophysical Properties of Matter)* (New York: Plenum)
[14] Ingel R P and Lewis D 1988 *J. Am. Ceram. Soc.* **71** 265
[15] Shimojo F and Okazaki H 1992 *J. Phys. Soc. Japan* **61** 4106
[16] Kisi E H and Howard C J 1998 *Zirconia Engineering Ceramics: Old Challenges—New Ideas (Key Engineering Materials Series)* ed E H Kisi (Zurich: Trans Tech) at press